Preliminary Report

Pages 1–4
2021

Signatures of Chaos in the Winds of Wolf-Rayet Stars

N.M. Khang, L. Shi, I. Stevens

MSci Physics with Astrophysics

School of Physics and Astronomy, University of Birmingham

17/12/2021

Keywords: Wolf-Rayet Stars, Time Series, Light Curves, Periodicity, Chaos

1 INTRODUCTION

Wolf-Rayet stars (WRs) are extremely massive stars ($\approx 10 - 25 M_{\odot}$, Crowther (2007)) with a very high mass loss rate via its stellar wind. Its fast and dense stellar wind is of utmost importance to stellar evolution and star formations. Most notably, it helps to drive and quench star formations by ionising H_{II} regions and dispersing leftover gas from the star forming processes (Rate and Crowther, 2020). However, that makes them very unstable by nature and presents a myriad of instabilities in their wind.

In this project we will be investigating a sample of bright WR stars observed with the NASA TESS satellite. Our primary goal is to characterise the nature of the variability of these WRs and look for signatures of low-order chaos that could be expected to arise in their violent winds. In addition to characterising their light curves, we will investigate the winds even further by using tools and techniques from non-linear dynamics such as mutual information, permutation entropy, Lyapunov exponents, etc..

2 DATA

The data was mainly obtained from the online Galactic Wolf Rayet Catalogue compiled by Rosslowe and Crowther (2015), which contains all the known galactic WR stars for us to work with. The entirety of the catalogue contains a total of 760 known sources.

We only select the brightest WRs to work with in this project, and hence applied onto the downloaded catalogue a filter for stars which have $V < 12$. This narrowed the list down to only 89 WRs. Since we are working with TESS time series data, we then further refine the list by utilising the Web TESS Viewing Tool (WTV) to investigate the sectors at which each of these stars are observed by the TESS satellite. We then search for their available 2-minute cadence data via the MAST archive with a search radius of 60 arcsec. Because of this method, we are bound to have multiple targets observed within the search radius. Therefore, we only select targets which are detected within the smallest radii as those are more likely to be our desired samples. Table 1 details our final finding of all WRs which have 2-minute TESS cadence data.

In this preliminary report, we are mainly showcasing our time series analysis of WR6, WR3 and WR40 to demonstrate the differences in their behaviours and why they are interesting starting points to our research project. We will use the PDCSAP (Pre-search Data Conditioning Simple Aperture Photometry) flux as it is the more carefully treated than the SAP flux as this method attempts to remove systematic artifacts from the signal. We are extracting and treating these datasets using the Python library *lightkurve*.

3 PRELIMINARY RESULTS

3.1 WR6

WR6 is one of the brightest (and more well-known) Wolf-Rayet star and is also known to be a binary system. Its apparent magnitude varies over a the course of roughly 3.7 days which is measured by St-Louis et al. (1995).

Interestingly, when we inspect the Lomb-Scargle periodogram for the three light curve data that TESS has on this target, we found that only the third data set has a period-at-max-power close to 3.7 days, whilst the first two datasets' returns a max-power period of roughly 1.8 days instead. We suspect that this might be due to the system's binarity that is causing this, or it might be due to the system's stellar winds that is causing this shift in its measured spectral variation period.

Regardless of this observation, we then proceeded to fold each of these periodograms by multiplying its period-at-max-power by 4 and applying a wrapping phase of 0.2. The result of one of the light curve is shown in Figure 2, where we can distinctly see its periodic behaviour. The other light curves' results also had similar outcomes with clear indications of a regular period in its spectral variation.

In short, WR6 is a relatively tame Wolf-Rayet star in terms of measured flux period, which makes it a good non-chaotic candidate in our research project.

We then tried our hands at characterising its light curve by fitting its periodogram, using a Markov Chain Monte Carlo (MCMC) method via *emcee* (Foreman-Mackey et al., 2013), to an amplitude spectrum function of the form given by Bowman et al. (2019) as,

$$\alpha(\nu) = \frac{\alpha_0}{1 + (\frac{\nu}{\nu_{\text{char}}})^{\gamma}} + C_w \tag{1}$$

where α_0 represents zero-frequency amplitude, γ is the logarithmic amplitude gradient, ν_{char} is the characteristic frequency which varies inversely to the characteristic timescale such that $\nu_{\text{char}} = (2\pi\tau)^{-1}$, and C_w is a frequency-independent white noise term (Blomme et al., 2011).

This remains an on-going objective as we are trying to finding solutions to use *emcee* correctly to do the Bayesian analysis and fitting of the periodogram. We might experiment with another Bayesian analysis library called *dynesty* (Speagle, 2020) if need be.

3.2 WR3 & WR40

In stark contrast to what is shown in WR6, the results obtained in analysing these two Wolf-Rayet stars' light curves are much more unpredictable. Their folded periodograms in Figure 2 showed two very different behaviours in both WR3 and WR40 compared to each other and compared to WR6.

WR3's flux measurements are a whole order of magnitude below either WR6 or WR40. This makes the plot appear very fuzzy as it is heavily affected by noise, making the job of distinguishing a period out of it much more difficult. This suggest that for WRs like WR3, we would need more

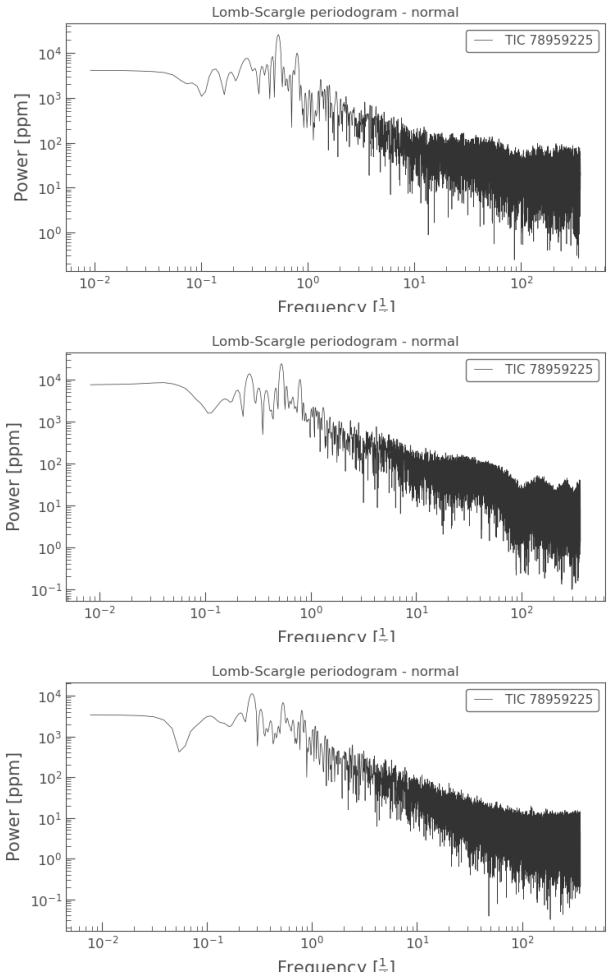

Fig. 1. Lomb-Scargle periodograms of 3 measured light curves of specifically WR6. The top two shows the period at max power to be around 1.8 days, however the bottom plot's max-power period is around 3.7 days, which is supposed to be its true value (St-Louis et al., 1995)

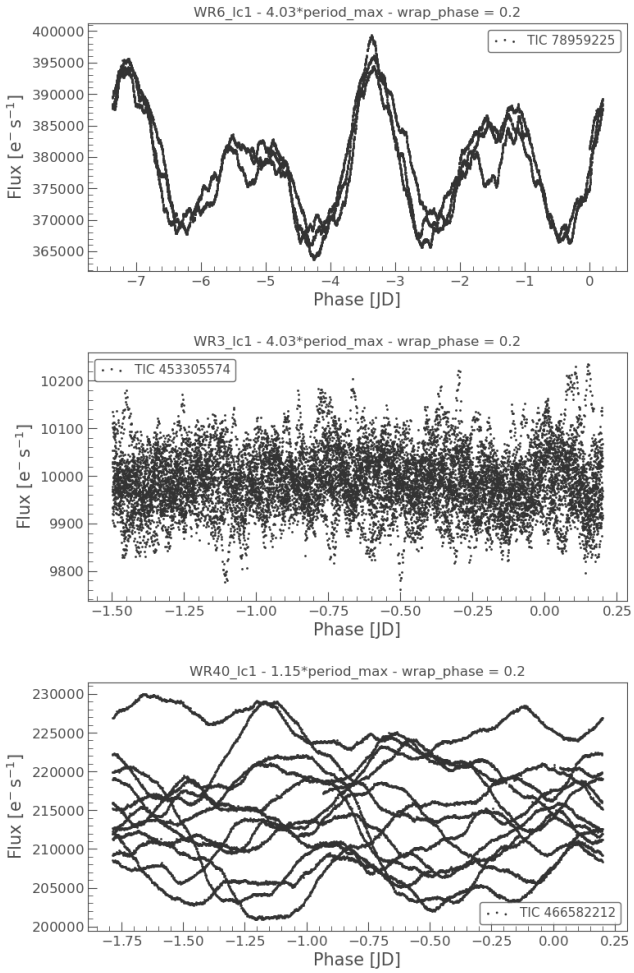

Fig. 2. Folded periodograms of WR6 (*top*), WR3 (*middle*) and WR40 (*bottom*). Fold parameters are given in each plot's titles.

work on cleaning the data before we can extract any meaningful science out of it.

For WR40, however, its spectral flux period are highly unpredictable and most likely is chaotic (Ramiaramanantsoa et al., 2019). There are no recognisable patterns in its measurements even prior to folding the period. This presents us with a unique candidate that is of promise when we get to the latter stages of this project, where we start to characterise and exploring signs of chaos within these WRs' light curves, and especially of those similar to WR40.

4 DISCUSSIONS & FUTURE PLANS

With our current results, it is too early to start making judgements on whether a signal shows (non-)chaotic behaviours or not.

In Semester 2, our focus will primarily lie in the characterisations of the obtained light curves. Prior to that, my target is to be able to successfully utilise the Bayesian MCMC framework via the Python code *emcee* (Foreman-Mackey et al., 2013) to fit my Lomb-Scargle periodogram of WR6 with Equation 1. Upon which, these best fit parameters allow for characterising the stochastic, low-frequency variability of WR6.

These can then serve as the basis to which I will move on to using different tools to characterise these star's light curves. By using the characteristic timescale, τ, one can start working on the recurrence analysis of the star's time series as it can tell us information about the dynamical nature of our sources, and providing glimpses of the origins of these light curves themselves (Robinson and Thiel, 2009; Phillipson et al., 2020). We will also be utilising a non-linear time series software called *TISEAN* (Hegger et al., 1999) and following similar methods applied by Phillipson et al. (2018, 2020) to further delve into complicated dynamical WR systems in our selected dataset in Table 1. We would also like to be moving onto testing out chaos decision trees (Toker et al., 2019) for the detection of chaos in noisy measurements which can be beneficial for systems similar to WR3. Permutation entropy and artificial neural networks (ANNs) are also immensely useful approaches, as described by Boaretto et al. (2021), to distinguish which set of WRs have time series data that are either chaotic or stochastic. If time permitting, we might even venture out to obtain 30-min cadence data of our WRs from their TESS FFI frames for our project.

WR#	Reference	HD	RA	DEC	Spectral Type	U	B	V	G	J	H	K	Distance	DistanceRef	LC_no
1	VII	HD 4004	00 43 28.39	+64 45 35.4	WN4b	10.36	10.74	10.1	9.79	8.206	7.857	7.48	3.15	RC20	0
2	VII	HD 6327	01 05 23.03	+60 25 18.9	WN2b	11.04	10.35	10.99		10.036	9.783	9.445	2.4	CSM19	0
3	VII	HD 9974	01 38 55.62	+58 09 22.6	WN3ha	9.85	10.62	10.61	10.58	10.237	10.134	10.009	2.9	RC20	1
4	VII	HD 16523	02 41 11.67	+56 43 49.8	WC5+?	10.03	10.3	9.8	9.68	8.749	8.566	7.877	3.75	RC20	1
5	VII	HD 17638	02 52 11.66	+56 56 07.1	WC6	10.97	10.85	10.37	10.06	8.626	8.336	7.653	2.97	RC20	0
6	VII	HD 50896	06 54 13.04	-23 55 42.0	WN4b	5.64	6.6	6.87	6.57	6.353	6.226	5.893	2.27	RC20	3
7	VII	HD 56925	07 18 29.13	-13 13 01.5	WN4b	11.21	11.68	11.4	11.17	9.97	9.674	9.271	4.23	RC20	2
8	VII	HD 62910	07 44 58.22	-31 54 29.5	WN7o/CE	10.08	10.69	10.16	9.92	8.57	8.322	7.928	3.74	RC20	0
9	VII	HD 63099	07 45 50.40	-34 19 48.5	WC5+O7	11.47	11.42	10.49	10.14	8.452	8.11	7.545	4.57	RC20	1
10	VII	HD 65865	07 59 46.24	-28 44 03.0	WN5h	10.62	11.22	10.93	10.94	10.053	9.887	9.61	5.46	RC20	1
11	VII	HD 68273	08 09 31.96	-47 20 11.8	WC8+O7.5III-V	0.64	1.58	1.83	1.7	2.15	2.25	2.1	0.34	vL07	4
12	VII		08 44 47.29	-45 58 55.4	WN8h	10.95	11.34	10.78	10.36	8.616	8.26	7.869	5.71	RC20	2
14	VII	HD 76536	08 54 59.16	-47 35 32.6	WC7+?	8.96	9.44	8.92	8.61	7.486	7.245	6.612	2.22	RC20	2
15	VII	HD 79573	09 13 11.76	-50 06 25.5	WC6	12.3	11.8	10.69	10.16	7.846	7.338	6.596	2.96	RC20	2
16	VII	HD 86161	09 54 52.89	-57 43 38.2	WN8h	7.94	8.63	8.32	8.05	6.968	6.714	6.38	2.63	RC20	2
17	VII	HD 88500	10 10 31.90	-60 38 42.4	WC5		10.87	10.63	10.42	9.926	9.736	9.167	6.75	RC20	2
18	VII	HD 89358	10 17 02.26	-57 54 46.8	WN4b	11.1	11.26	10.75	10.34	8.566	8.205	7.676	3.82	RC20	2
21	VII	HD 90657	10 26 31.40	-58 38 26.1	WN5o+O4-6; WN5o+O7V	9.53	10.16	9.71	9.49	8.414	8.217	8.033	3.99	rc20	2
22	VII	HD 92740	10 41 17.50	-59 40 36.8	WN7ha; WN7h+O9III-V	5.69	6.48	6.39	6.23	5.705	5.578	5.389	2.33	RC20	3
23	VII	HD 92809	10 41 38.31	-58 46 18.7	WC6	9.02	9.51	9.11	8.87	7.889	7.602	7.055	2.55	RC20	2
24	VII	HD 93131	10 43 52.24	-60 07 04.0	WN6ha	5.52	6.46	6.48	6.35	6.097	6.012	5.816	3.55	RC20	3
25	VII	HD 93162	10 44 10.37	-59 43 11.1	O2.5If*/WN6+O	7.9	8.51	8.07	7.79	6.26	5.97	5.721	1.97	RC20	3
31	VII	HD 94546	10 53 44.81	-59 30 46.6	WN4o+O8V	10.38	10.95	10.56	10.39	9.172	8.962	8.688	6.11	RC20 (n flag)	1
31a	VII		10 53 59.57	-60 26 44.3	WN11h		11.64	10.85	10.27	7.323	6.719	6.097	7.35	RC20	0
31b	VII	HD 94910	10 56 11.57	-60 27 12.8	WN11h	7	7.74	7.21	7.32	5.42	5.084	4.531	4.85	RC20	0
40	VII	HD 96548	11 06 17.20	-65 30 35.3	WN8h	7.1	7.86	7.69	7.46	6.622	6.407	6.107	3.83	RC20	3
42	VII	HD 97152	11 10 04.07	-60 58 44.9	WC7+O7V	7.44	8.18	8.05	7.92	7.589	7.519	7.084	2.44	RC20	1
43A	VII	HD97950 A1	11 15 07.47	-61 15 38.16	WN6ha+WN6ha			11.18		7.98	7.79	7.21	7.6	MMM08	1
43B	VII	HD97950 B	11 15 07.58	-61 15 38.32	WN6ha		12.34	11.33		7.78	7.7	7.08	7.6	MMM08	1
43C	VII	HD 97950 C	11 15 07.76	-61 15 37.75	O3If*/WN6		12.94	11.89		8.49	8.13	7.81	7.6	MMM08	1
46	VII	HD 104994	12 05 18.71	-62 03 10.1	WN3b pec	9.95	10.77	10.58	10.7	10.199	10.079	9.834	2.6	RC20	2
47	VII	HD 311884	12 43 50.99	-63 05 14.8	WN6o+O5V; WN6o+O5.5	11.39	11.59	10.79	10.29	8.316	7.916	7.549	3.49	RC20	2
	...	...	...	...	...	...	...	...	...	...	...	...	...	...	...
155	VII	HD 214419	22 36 53.95	+56 54 20.9	WN6o+O9II-Ib	8.44	9.26	8.83	8.71	7.482	7.34	7.161	2.99	RC20	1
157	VII	HD 219460	23 15 12.39	+60 27 01.8	WN5o(+B1II)	10.72	11.11	10.5	10.26				2.57	RC20	0
158	VII		23 43 30.59	+61 55 48.1	WN7h	12.02	12.2	11.24	10.71	8.638	8.201	7.811	5	RC20	0
159	VIIA		23 47 20.38	+63 13 14.2	WN4			11.2	10.53				1.82	RC20	0

Table 1. Table of 78 TESS-observed Wolf-Rayet stars. This table only shows an excerpt of a few dozen stars for demonstrations, the full table can be found here. Photometry measurements in U, B, V, J, H, K are done in the Johnson system, whilst the G-band is done by Gaia. The last column named "LC_no" indicates how many light curve measurements are available for each WR star. We decided to retain some targets with no 2-minute cadence data, because since they are observed by TESS, it is possible to extract their data perhaps with a longer cadence

REFERENCES

R. Blomme, L. Mahy, C. Catala, J. Cuypers, E. Gosset, M. Godart, J. Montalban, P. Ventura, G. Rauw, T. Morel, P. Degroote, C. Aerts, A. Noels, E. Michel, F. Baudin, A. Baglin, M. Auvergne, and R. Samadi. Variability in the CoRoT photometry of three hot O-type stars. HD 46223, HD 46150, and HD 46966. , 533:A4, September 2011. doi: 10.1051/0004-6361/201116949.

B. R. R. Boaretto, R. C. Budzinski, K. L. Rossi, T. L. Prado, S. R. Lopes, and C. Masoller. Discriminating chaotic and stochastic time series using permutation entropy and artificial neural networks. *Scientific Reports*, 11:15789, August 2021. doi: 10.1038/s41598-021-95231-z.

Dominic M. Bowman, Siemen Burssens, May G. Pedersen, Cole Johnston, Conny Aerts, Bram Buysschaert, Mathias Michielsen, Andrew Tkachenko, Tamara M. Rogers, Philipp V. F. Edelmann, Rathish P. Ratnasingam, Sergio Simón-Díaz, Norberto Castro, Ehsan Moravveji, Benjamin J. S. Pope, Timothy R. White, and Peter De Cat. Low-frequency gravity waves in blue supergiants revealed by high-precision space photometry. *Nature Astronomy*, 3:760–765, May 2019. doi: 10.1038/s41550-019-0768-1.

Paul A. Crowther. Physical Properties of Wolf-Rayet Stars. , 45(1):177–219, September 2007. doi: 10.1146/annurev.astro.45.051806.110615.

Daniel Foreman-Mackey, David W. Hogg, Dustin Lang, and Jonathan Goodman. emcee: The MCMC Hammer. , 125(925):306, March 2013. doi: 10.1086/670067.

Rainer Hegger, Holger Kantz, and Thomas Schreiber. Practical implementation of nonlinear time series methods: The TISEAN package. *Chaos*, 9(2):413–435, June 1999. doi: 10.1063/1.166424.

R. A. Phillipson, P. T. Boyd, and A. P. Smale. The chaotic long-term X-ray variability of 4U 1705-44. , 477(4):5220–5237, July 2018. doi: 10.1093/mnras/sty970.

R. A. Phillipson, P. T. Boyd, A. P. Smale, and M. S. Vogeley. Complex variability of Kepler AGN revealed by recurrence analysis. , 497(3): 3418–3439, September 2020. doi: 10.1093/mnras/staa2069.

Tahina Ramiaramanantsoa, Richard Ignace, Anthony F. J. Moffat, Nicole St-Louis, Evgenya L. Shkolnik, Adam Popowicz, Rainer Kuschnig, Andrzej Pigulski, Gregg A. Wade, Gerald Handler, Herbert Pablo, and Konstanze Zwintz. The chaotic wind of WR 40 as probed by BRITE. , 490(4):5921–5930, December 2019. doi: 10.1093/mnras/stz2895.

Gemma Rate and Paul A. Crowther. Unlocking Galactic Wolf-Rayet stars with Gaia DR2 - I. Distances and absolute magnitudes. , 493(1): 1512–1529, March 2020. doi: 10.1093/mnras/stz3614.

Geoffrey Robinson and Marco Thiel. Recurrences determine the dynamics. *Chaos*, 19(2):023104, June 2009. doi: 10.1063/1.3117151.

C. K. Rosslowe and P. A. Crowther. Spatial distribution of Galactic Wolf-Rayet stars and implications for the global population. , 447(3):2322–2347, March 2015. doi: 10.1093/mnras/stu2525.

Joshua S. Speagle. DYNESTY: a dynamic nested sampling package for estimating Bayesian posteriors and evidences. , 493(3):3132–3158, April 2020. doi: 10.1093/mnras/staa278.

Nicole St-Louis, M. J. Dalton, S. V. Marchenko, A. F. J. Moffat, and A. J. Willis. The IUE MEGA Campaign: Wind Structure and Variability of HD 50896 (WN5). , 452:L57, October 1995. doi: 10.1086/309706.

Daniel Toker, Friedrich T. Sommer, and Mark D'Esposito. A simple method for detecting chaos in nature. *arXiv e-prints*, art. arXiv:1904.00986, March 2019.